

# Natural orbitals and two-particle correlators as tools for analysis of effective exchange couplings in solids

Pavel Pokhilko<sup>1</sup> and Dominika Zgid<sup>1,2</sup>

<sup>1</sup>*Department of Chemistry, University of Michigan, Ann Arbor, Michigan 48109, USA*

<sup>2</sup>*Department of Physics, University of Michigan, Ann Arbor, Michigan 48109, USA*

Using generalizations of natural orbitals, spin-averaged natural orbitals, and two-particle charge correlators for solids, we investigate electronic structure of antiferromagnetic transition-metal oxides with a fully self-consistent, finite-temperature GW method. Our findings disagree with Goodenough–Kanamori (GK) rules, commonly used for qualitative interpretation of such solids. First, we found a strong dependence of natural orbital occupancies on momenta contradicting GK assumptions. Second, along the momentum path, the character of natural orbitals changes. In particular, contributions of oxygen 2s orbitals are important, which has not been considered in the GK rules. To analyze the influence of electronic correlation on the values of effective exchange coupling constants, we use both natural orbitals and two-particle correlators and show that electronic screening modulates the degree of superexchange by stabilizing the charge-transfer contributions, greatly affecting these coupling constants. Finally, we give a set of predictions and recommendations regarding the use of density functional, Green’s function, and wave-function methods for evaluating effective magnetic couplings in molecules and solids.

## I. INTRODUCTION

The wave function employed in the description of magnetic phenomena requires multiple configurations to quantitatively and qualitatively describe magnetic states. Since the treatment of both strong and weak electron correlation is necessary, a number of strategies for evaluation of molecular magnetic couplings has been used in the past. Among the active-space wave-function methods, various selective and multireference configuration interaction[1, 2] and perturbation theories[3–5] are commonly used for small molecules where such calculations are affordable. While strong correlation is important for the description of magnetic interactions, explicit multireference methods are not the only family of approaches that can accurately capture it. For example, magnetic couplings can also be efficiently and accurately computed within spin-flip family of methods[6] that includes several spin-flip time-dependent density functional theory (SF-TDDFT) formulations[7–18] and equation-of-motion coupled-cluster methods[19, 20] (EOM-SF-CC) or its perturbative approximations[21]. Broken-symmetry approaches form another family of methods that when combined with DFT (denoted as BS-DFT) are the most common tools for evaluating magnetic couplings due to their low computational cost. Broken-symmetry approaches have also been deployed within a number of wave-function[22–24] and Green’s function methods[25–27]. Another approach is to use a magnetic force theorem[28], which is even cheaper than BS-DFT when deployed within DFT[29].

For solids, due to high computational cost and necessity of reaching solutions in thermodynamic limit (to remove finite-size effects), the evaluation of magnetic couplings within the wave-function formalism was rarely performed before[30–32]. The majority of magnetic

exchange calculations in solids was performed using BS-DFT. However, BS-DFT has numerous disadvantages. First, it depends on a particular functional parametrization (in the Kohn–Sham formulation); thus, it is not systematically improvable. Second, the extraction procedure of magnetic couplings from the BS-DFT solutions is not well defined and a number of approximate spin-projection and decontamination schemes have been employed[33–36] in the past. Moreover,  $\langle S^2 \rangle$  needed for such spin projections often is not evaluated rigorously within DFT[37–39], which ultimately introduces additional errors. Analysis of spin contamination in solids is even more complicated and is based on various spin–spin correlation functions[27, 40].

Green’s function methods[41–43] offer a viable and affordable alternative for treating magnetic phenomena in solids. On one hand, unlike bulky multi-index wave-function amplitudes, the one-electron Green’s function depends only on two orbital and one time index resulting in a very compact object suitable for the development of computationally efficient methods. On the other hand the Green’s function and self-energy contain a lot of information about the system and can be used to evaluate one- and some of the two-particle observables directly. Due to these features, these powerful methods found numerous applications in, for instance, in photoelectron spectroscopy[44–46] and superconductivity[47].

Fully self-consistent Green’s function methods do not depend on any adjustable parameters and have a systematically improvable perturbative expansion given by skeleton (bold) diagrams[48]. The Green’s function methods based on such a bold diagrammatic expansion are also called conserving, since for them the Kadamoff–Baym theorem[49, 50] grants the conservation of momentum, angular momentum, energy as well as gauge invariance of the Luttinger–Ward functional and the current continuity. Full self-consistency removes any dependence on a starting point, which is not removed within the non-self-consistent and partly self-consistent methods. Recently, we have introduced an  $\langle S^2 \rangle$  evaluation in the self-consistent Green’s function formalism[51] and found that in many cases the degree of spin contamination between different magnetic solutions in molecules[26] and solids[27] is very small, making the extraction procedure rigorous, unambiguous, and simple.

Effective Hamiltonian theory[52–56] offers a straightforward way for constructing magnetic Hamiltonians. This theoretical framework has been used within a number of methods[57, 58] both for the derivation purposes as well as for constructing new approximations based on the physics of the effective Hamiltonians[59–63]. Another but related strategy utilizes finite-order perturbative expansions of effective Hamiltonians and investigates configurations contributing to the effective exchange coupling. For example, Kramers[64] and Anderson[65] used the latter strategy, and classified various terms into direct exchange, kinetic exchange, and spin-polarisation terms[66, 67]. Unfortunately, such terminology is often misleading since these terms are defined differently in various publications. Such an analysis (sometimes emphasized as an exchange decomposition) has been less rigorously extended to BS-DFT[68–71], where such terms are defined through “energies” of various unoptimized, partly optimized, and fully optimized restricted open-shell determinants with approximate spin projections. Besides ambiguity, an apparent limitation of this decomposition is in its strong dependence on a particular family of methods, making it not applicable for the analysis and comparisons of magnetic couplings between various electronic structure methods.

A robust analysis shall probe the nature of the system *directly* and without any dependence on a particular flavor of electronic structure method. For example, natural orbitals and two-particle correlators provide such an ansatz-agnostic analysis, which made them applicable for both wave-function and Green’s function methods[26]. This unified language

not only gives an insight into basic physics of the particular system, but also allows one to look at electronic structure from different perspectives and to establish deeper connections between different families of methods.

In this paper, we extend the analysis of molecular electronic structure based on natural orbitals and two-particle charge correlators to solids and deploy it within Green's function methods. Such a generalization allows us to quantify and analyze the location of open-shell electrons, the degree of open-shell and charge-transfer nature, and the role of electron correlation in transition-metal oxides—systems with a substantial presence of superexchange. Based on this analysis, we gain a deeper insight into the physics of magnetic interactions and formulate physical predictions that can be checked numerically in the future.

## II. THEORY

### A. Green's functions and density matrices

We choose to work with Bloch orbitals since they allow us to directly *translate* electronic structure methods from molecules to solids. In the same way, one can also transfer the analysis of electronic structure, which we pursue in this paper. The Bloch orbitals are defined as

$$\phi_{\mathbf{k},i} = \sum_{\mathbf{R}} \phi_i^{\mathbf{R}}(\mathbf{r}) e^{i\mathbf{k}\cdot\mathbf{R}}, \quad (1)$$

where  $\mathbf{k}$  is the momentum vector index,  $i$  subscript enumerates atom-centered combination of primitive Gaussians  $\phi_i^{\mathbf{R}}(\mathbf{r})$  in the unit cell,  $\mathbf{R}$  is a Bravais lattice position,  $\mathbf{r}$  is the space electronic coordinate. For convenience, we merge spin, momentum, and space coordinates[72] and label the corresponding momentum-dependent spin-orbitals with multi-indices:  $\mathbf{p}, \mathbf{q}, \mathbf{r}, \mathbf{s}$ . Such notation is very compact and analogous to the molecular case, making generalizations to solids transparent. For example, one-particle Green's functions[41–43] are defined as

$$G_{\mathbf{p}\mathbf{q}}(\tau) = -\frac{1}{Z} \text{Tr} \left[ e^{-(\beta-\tau)(\hat{H}-\mu\hat{N})} a_{\mathbf{p}} e^{-\tau(\hat{H}-\mu\hat{N})} a_{\mathbf{q}}^{\dagger} \right], \quad (2)$$

$$Z = \text{Tr} \left[ e^{-\beta(\hat{H}-\mu\hat{N})} \right], \quad (3)$$

where  $\mathbf{p}, \mathbf{q}$  subscripts label the momentum-dependent spin-orbitals,  $a_{\mathbf{p}}$  and  $a_{\mathbf{q}}^{\dagger}$  operators are the second-quantized annihilation and creation operators for the corresponding momentum-dependent spin-orbital representation,  $\tau$  is the imaginary time,  $\hat{H}$  is the electronic Hamiltonian in the second-quantized representation,  $\hat{N}$  is the particle-number operator,  $\mu$  is the chemical potential,  $\beta$  is the inverse temperature,  $\text{Tr}$  is the matrix trace taken in the space of all possible configurations in the Fock space,  $Z$  is the grand-canonical partition function.

Because of the momentum conservation, the Green's function matrix is block-diagonal in the momentum space and the only non-zero blocks  $G_{pq}^{\mathbf{k}}$  can be labeled with a single momentum index. The orbitals used for expressing the Green's function and self-energy matrix elements do not have to be orthogonal, which allows us to use atomic orbitals (AO) directly in the implementation. In this work, we use only unrestricted orbital choice (as in unrestricted Hartree–Fock method, UHF), where the non-zero (and possibly different) spin

blocks are  $\alpha\alpha$  and  $\beta\beta$ , while  $\alpha\beta$  and  $\beta\alpha$  blocks are zero[73]. Originally, the imaginary-time formalism (also known as the Matsubara formalism) was designed for the description of thermal phenomena[41–43]. Although all the analysis performed in this paper is formally temperature-dependent, the symmetry-broken Green’s function solutions do not change significantly in the broad temperature range, effectively corresponding to the zero-temperature limit. The details of this behavior are explained in Ref.26.

The one-particle density matrix  $\gamma$  expressed in spin orbitals and any one-electron observable  $A = \sum_{\mathbf{p}\mathbf{q}} A_{\mathbf{p}\mathbf{q}} a_{\mathbf{p}}^\dagger a_{\mathbf{q}}$  can be accessed directly from the imaginary-time Green’s function:

$$\gamma_{\mathbf{p}\mathbf{q}} = -G_{\mathbf{q}\mathbf{p}}(\tau = 0^-) \quad (4)$$

$$\langle A \rangle = \sum_{\mathbf{p}\mathbf{q}} A_{\mathbf{p}\mathbf{q}} \gamma_{\mathbf{p}\mathbf{q}}. \quad (5)$$

Note that the one-electron operator  $A$  can be a particle-number operator with the corresponding integrals  $A_{\mathbf{p}\mathbf{q}} = S_{\mathbf{p}\mathbf{q}}$ , which are just orbital overlaps. Since in solids evaluation of  $\langle A \rangle$  per unit cell is often the objective, a division by the volume of the Brillouin zone is necessary as in Eqs. 11 and 12. Because of its simplicity and ansatz-agnostic nature, the analysis of density matrices have been used to understand a broad range of aspects of molecular electronic structure through various orbital representations (a far from a complete list of references can be found in Refs[74–91]). For the analysis of magnetic effective exchange couplings, various orbital choices have been used[92], including natural orbitals[17, 18, 26, 93–96]. While the most common selection of magnetic orbitals is based on single occupied molecular orbitals, such orbitals are often too delocalized to represent magnetic physics, while the natural orbitals remain compact and insightful[17].

Natural orbitals (NO) for molecules are defined as the eigenvectors of one-particle density matrix; their occupancies are the corresponding eigenvalues. One may diagonalize a particular spin block of the density matrix and obtain natural spin-orbitals or one can diagonalize the spin-averaged density matrix ( $\gamma_{\alpha\alpha} + \gamma_{\beta\beta}$ ) and obtain spin-averaged natural orbitals (SA-NO). We directly generalize these concepts to solids as

$$\gamma_{\sigma\sigma} \phi_{\mathbf{k},i,\sigma}^{NO} = d_{\mathbf{k},i,\sigma} \phi_{\mathbf{k},i,\sigma}^{NO} \quad (6)$$

$$(\gamma_{\alpha\alpha} + \gamma_{\beta\beta}) \phi_{\mathbf{k},i}^{SA-NO} = d_{\mathbf{k},i} \phi_{\mathbf{k},i}^{SA-NO}, \quad (7)$$

where  $\phi_{\mathbf{k},i,\sigma}^{NO}$  and  $\phi_{\mathbf{k},i}^{SA-NO}$  are the corresponding natural and spin-averaged natural momentum-dependent orbitals,  $d$  denotes their occupation numbers, and the multi-index dependence is expanded explicitly for clarity. Because of the momentum dependence, such NOs are extended waves if plotted in the real space. To our knowledge, only plane-wave NOs (but not the Bloch NOs as in the eq.1) have previously been used in periodic calculations[97, 98].

Occupancies of natural orbitals can serve to identify open-shell electrons. For the cases where a clear separation between doubly occupied, singly occupied, and virtual orbitals is not achieved, a number of metrics has been introduced in the past. In this work, we use the linear  $n_l$  and non-linear  $n_{nl}$  indices from the Refs.[99, 100], which are sometimes called

Yamaguchi and Head-Gordon indices, respectively

$$n_l = \sum_p \min(d_p, 2 - d_p),$$

$$n_{nl} = \sum_p d_p^2 (2 - d_p)^2,$$

where  $d_p$  is an occupancy of SA-NO. To investigate the open-shell magnetic structure in solids, we generalize these indices for  $\mathbf{k}$ -dependent SA-NOs:

$$n_{l,\mathbf{k}} = \sum_p \min(d_{\mathbf{k},p}, 2 - d_{\mathbf{k},p}),$$

$$n_{nl,\mathbf{k}} = \sum_p d_{\mathbf{k},p}^2 (2 - d_{\mathbf{k},p})^2.$$

Imaginary-time-dependent quantities can also be Fourier transformed to a frequency representation. Such a set of frequencies is discrete and is called Matsubara frequencies. They are defined respectively for the fermionic and bosonic quantities as:

$$\omega_n = \frac{(2n + 1)\pi}{\beta}, \quad (8)$$

$$\Omega_n = \frac{2n\pi}{\beta}. \quad (9)$$

In the fully self-consistent GW, during each of the iterations, we solve the Dyson equation:

$$G^{-1}(i\omega_n) = G_0^{-1}(i\omega_n) - \Sigma[G](i\omega_n), \quad (10)$$

where  $G$  is the full one-particle Green's function,  $G_0$  is the Green's function of independent electrons, and  $\Sigma[G]$  is the self-energy that has a functional dependence only on the full Green's function  $G$  and two-electron integrals. The self-energy encodes all the orbital relaxation, screening, and correlation effects. In particular, fully self-consistent approximations are based on perturbative expansions of the self-energy, preserving the functional dependence on  $G$  and the two-electron integrals. The simplest example of the such an approximation is the Hartree–Fock theory. In the notation above, the Hartree–Fock self-energy is only static (does not depend on time) and is a part the Fock matrix times minus one. Correlated post-Hartree–Fock methods have an additional dynamical part of the self-energy, describing correlation and screening.

In this work, we use the fully self-consistent GW approximation[101–110]. The theoretical and implementation details for solids are fully covered in Refs.[109, 110].

The imaginary time dependence of the Green's function and self-energy are very important since they provide a route for evaluating properties and electronic energy. For example,

electronic energy is evaluated from the Galitskii–Migdal expression as

$$E_{1b} = \frac{1}{V_{BZ}} \sum_{pq} h_{pq}^{\mathbf{k}} \gamma_{pq}^{\mathbf{k}}, \quad (11)$$

$$E_{2b} = \frac{1}{2V_{BZ}\beta} \sum_{\omega_n} \sum_{pq} G_{qp}^{\mathbf{k}}(\omega_n) \Sigma_{pq}^{\mathbf{k}}(\omega_n), \quad (12)$$

where  $h_{\mathbf{p}\mathbf{q}}$  are one-electron integrals,  $V_{BZ}$  is the volume of a Brillouin zone,  $E_{1b}$  and  $E_{2b}$  are the one- and two-body parts of the total energy.

Analysis based on NOs has some limitations. It can give insights only into the structure of the one-particle density matrix, but not into the two-particle observables. This limitation explains why NOs are not sufficient for a complete understanding of energy differences and, therefore, effective exchange couplings. To mitigate this issue, we also include two-particle observables in our analysis. Recently, we applied the thermodynamic Hellmann–Feynman theorem and showed that for any fully self-consistent Green’s function method the two-particle density matrices have disconnected and connected parts[51]:

$$\Gamma_{\langle \mathbf{p}\mathbf{q}|\mathbf{r}\mathbf{s} \rangle} = \Gamma_{\langle \mathbf{p}\mathbf{q}|\mathbf{r}\mathbf{s} \rangle}^{\text{disc}} + \Gamma_{\langle \mathbf{p}\mathbf{q}|\mathbf{r}\mathbf{s} \rangle}^{\text{conn}}, \quad (13)$$

$$\Gamma_{\langle \mathbf{p}\mathbf{q}|\mathbf{r}\mathbf{s} \rangle}^{\text{disc}} = \gamma_{\mathbf{p}\mathbf{r}} \gamma_{\mathbf{q}\mathbf{s}} - \gamma_{\mathbf{p}\mathbf{s}} \gamma_{\mathbf{q}\mathbf{r}}. \quad (14)$$

Such two-particle density matrices fully reproduce two-particle part of the energy when a trace with integrals is taken:

$$E_{2b} = \frac{1}{V_{BZ}^2} \sum_{\mathbf{p}\mathbf{q}\mathbf{r}\mathbf{s}} \langle \mathbf{p}\mathbf{q}|\mathbf{r}\mathbf{s} \rangle \Gamma_{\langle \mathbf{p}\mathbf{q}|\mathbf{r}\mathbf{s} \rangle}. \quad (15)$$

The explicit expression for the connected part of the two-particle density matrix (also called an electronic cumulant) depends on a particular approximation used, but it is always a contraction between a 4-point vertex function (encoding effective interactions) and Green’s functions at all 4 points. The fully self-consistent GW cumulant[51] is defined as

$$\Gamma_{(\mathbf{p}_0\mathbf{q}_0|\mathbf{r}_0\mathbf{s}_0)}^{\text{GW conn}} = -\frac{1}{\beta} \sum_{\Omega_m} \sum_{\mathbf{p}\mathbf{q}\mathbf{r}\mathbf{s}} \Pi_{\mathbf{r}_0\mathbf{s}_0\mathbf{p}\mathbf{q}}(\Omega_m) W_{(\mathbf{p}\mathbf{q}|\mathbf{r}\mathbf{s})}(\Omega_m) \Pi_{\mathbf{r}\mathbf{s}\mathbf{p}_0\mathbf{q}_0}(\Omega_m), \quad (16)$$

where  $\Pi$  is a polarization function. The physical meaning of this expression becomes transparent if one generalizes it to the full two-particle Green’s function, describing propagation of two particles. When particles propagate in a medium, they interact with it; therefore, their propagators become renormalized. Propagation of two particles in the medium can happen either without interaction with each other (giving the disconnected terms) or with interaction with each other. The structure of such an interaction is described by the 4-point vertex function, which is just  $W$  for GW.

Due to the equivalence and possibility of evaluating the electronic energy using either frequency-dependent formalism (Galitskii–Migdal) or two-particle density matrix traced with the integrals, it is sufficient to investigate only one route. Consistently, with our previous work for molecules[26], we choose to investigate only local two-particle observables for solids. Kubo[111] introduced statistical cumulants of two operators  $\hat{X}$  and  $\hat{Y}$ , measuring their

covariance:

$$\langle \delta \hat{X} \delta \hat{Y} \rangle = \langle \hat{X} \hat{Y} \rangle - \langle \hat{X} \rangle \langle \hat{Y} \rangle = \langle (\hat{X} - \langle \hat{X} \rangle) (\hat{Y} - \langle \hat{Y} \rangle) \rangle. \quad (17)$$

In localized orbitals, the two-particle charge[112–118] and spin [27, 119–123] cumulants have been extensively used to quantify bond orders, charge-transfer, and covalent nature of electronic states, as well as magnetic properties. In this work, we extend the concept of a charge cumulant to solids. We define a local particle-number operator as

$$\hat{N}_A^{\mathbf{k}} = \sum_{pq \in A} S_{pq}^{\mathbf{k}} (a_{\mathbf{k},p,\alpha}^\dagger a_{\mathbf{k},q,\alpha} + a_{\mathbf{k},p,\beta}^\dagger a_{\mathbf{k},q,\beta}). \quad (18)$$

Similarly to spin correlators[27]  $SS_{AB}^{\mathbf{k}=0}$  and  $SS_{AB}$ , we introduce particle-number correlators  $NN_{AB}^{\mathbf{k}=0}$  and  $NN_{AB}$ :

$$NN_{AB}^{\mathbf{k}=0} = \langle \delta \hat{N}_A^{\mathbf{k}=0} \delta \hat{N}_B^{\mathbf{k}=0} \rangle, \quad (19)$$

$$NN_{AB} = \frac{1}{V_{BZ}} \sum_{\mathbf{k}} \langle \delta \hat{N}_A^{\mathbf{k}} \delta \hat{N}_B^{\mathbf{k}} \rangle. \quad (20)$$

Such correlators quantify charge fluctuations and covariances between localized subsets of orbitals  $A$  and  $B$ .  $NN_{AB}^{\mathbf{k}=0}$  measures charge covariances at a  $\Gamma$ -point ( $\mathbf{k} = 0$ );  $NN_{AB}$  measures charge covariances in the real-space representation between orbital subsets in the same unit cell. Both measures provide diagnostics of the charge-transfer magnitude for a given Green's function solution. Due to high computational cost of evaluating the connected component of the two-particle density matrix, we include it only for very few  $\mathbf{k}$ -points. In this work, we neglect the connected contribution from the cumulant and consider only the disconnected part. Such an approximation is permissible since GW is a weakly correlated method and the magnitude of the electronic cumulant is predicted to be rather small. Previously, we tested the validity of this assumption for spin correlators[27].

### III. RESULTS AND DISCUSSION

#### A. Computational details

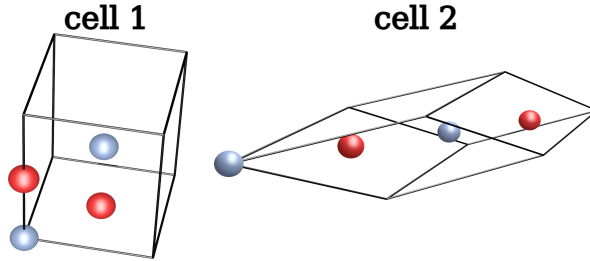


FIG. 1: Two supercells used in this paper to capture solutions of different types.

We performed calculations in the same manner as before in Ref. [27, 109]. We used *gth-dzvp-molopt-sr* basis set[124], *gth-pbe* pseudopotential[125], and *def2-svp-ri* auxiliary

basis[126] for the resolution-of-identity approximation (RI) of two-electron integrals. We used the rock-salt NiO, CoO, FeO structures with the lattice constants  $a = 4.1705\text{\AA}$  [127],  $4.2630\text{\AA}$  [128],  $4.285\text{\AA}$  [129], respectively. We used supercells of different types to capture solutions of different nature (Fig. 1). In each of the cells, we obtained ferromagnetic and antiferromagnetic broken-symmetry Green’s function solutions using frequency-dependent CDIIS algorithm for convergence acceleration from Ref.[130]. The GW calculations were started from the corresponding zero-temperature UHF solutions. We denote the ferromagnetic solutions with the highest spin projection as HS and the antiferromagnetic broken-symmetry solutions as BS. The Monkhorst–Pack k-point grid was used for the Brillouin-zone sampling[131]. The finite-size effects were accounted for within the exchange terms in UHF and GW with the probe-charge-corrected Ewald approach[132, 133]. All the frequency-dependent quantities were written in the intermediate representation[134] with  $\Lambda = 10^5$  and 136 functions. The one- and two-electron integrals were produced by the PySCF code[135]. RI was used for all the calculations performed with the local in-house Green’s function code [26, 51, 109, 110, 130, 136, 137]. Since we use very compact basis sets in solids, we used Mulliken-like partitioning of orbitals with simple AOs. Such a partitioning choice allows us to avoid costly integral transformations for solids. Natural orbitals are visualized with Gabedit 2.5.1[138] as isosurfaces with isovalues 0.050 and rendered with POV-Ray 3.7.0[139]. The  $k$ -path was constructed with ASE 3.22.0 package[140] and interpolated with Wannier interpolation in AOs. The largest eigenvalues of the interpolated density matrix slightly exceeded 2 at some k-points due to an imperfect interpolation; in such cases we capped these occupancies by 2 in the evaluation of  $n_l$  and  $n_{nl}$  indices. We use the symmetry convention for special points and for the  $k$ -path according to Ref. [141].

## B. Goodenough–Kanamori rules

In the compounds considered, the effective magnetic Hamiltonian[27, 30, 63, 142] has only non-zero couplings between the nearest neighbors  $J_1$  and between the next-nearest neighbors  $J_2$  and is expressed as

$$H = -J_1 \sum_{\langle i,j \rangle} \vec{S}_i \vec{S}_j - J_2 \sum_{\langle\langle i,j \rangle\rangle} \vec{S}_i \vec{S}_j. \quad (21)$$

Semiempirical Goodenough–Kanamori (GK) rules[143–145] are commonly used to explain the magnetic origin of effective interactions in transition-metal oxides and related compounds. They are based on simplistic models and assume localized interactions between orbitals and their overlaps. In particular, they consider the  $d - p - d$  bonds and show that the  $90^\circ$  angle between Ni–O–Ni results in a ferromagnetic interaction, while the  $180^\circ$  angle results in the antiferromagnetic interaction. With our tools for the analysis of electronic structure, we can check the validity of GK assumptions directly from electronic structure calculations without any additional approximations since natural orbitals can directly explain which orbitals are on average occupied by the open-shell electrons. Multielectron multi-center bonding from Ref.[146] provide an alternative description of magnetic interactions in terms of delocalized orbitals; natural orbitals directly generalize these ideas. Because of the local assumption, the GK rules predict that the open-shell electrons occupy orbitals with the same composition of atomic orbitals. As a result, all the corresponding NOs would be composed of  $d - p - d$  orbitals times the k-dependent phases with the same combinations

of AOs from the unit cell. In particular, such local contributions from nickel atoms in NiO are attributed to local  $t_{2g}$  atomic orbitals and contributions from oxygen are attributed exclusively to  $p$ -orbitals.

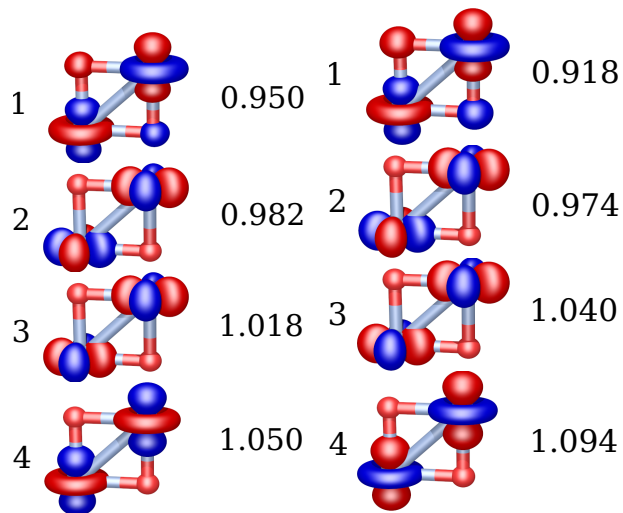


FIG. 2: SA-NOs and their occupancies computed for the broken-symmetry solutions at the  $\Gamma$  point of the NiO **cell 1** within UHF (left) and GW (right). The following atoms are pictured in the unit cell, starting from left top corner and moving clockwise, O-Ni-O-Ni. For every orbital, its number is shown on the left and its occupancy is shown on the right.

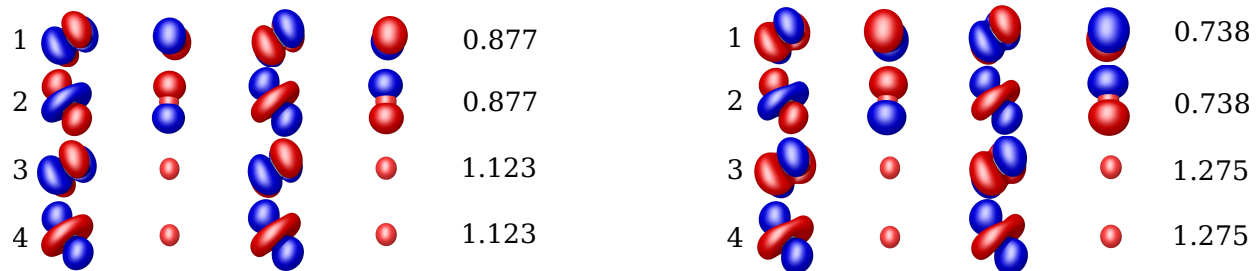


FIG. 3: SA-NOs and their occupancies computed for the broken-symmetry solutions at the  $\Gamma$  point of the NiO **cell 2** within UHF (left) and GW (right). To see a partly antibonding character of the d-p-d combinations, one can apply translations with respect to  $\mathbf{k} = 0$  wave, shown in Fig. S1 in SI. The following atoms are pictured in the unit cell, starting from left to right, Ni-O-Ni-Ni. For every orbital, its number is shown on the left and its occupancy is shown on the right.

### C. Natural orbitals at $\Gamma$ point

However, the computed natural orbitals show a different picture. The frontier spin-averaged natural orbitals with occupancies close to 1 are separated well from the doubly occupied and virtual SA-NOs. The frontier SA-NOs of NiO computed with UHF and GW for the broken-symmetry solutions at a  $\Gamma$  point are shown in Figs 2 and 3 for **cell 1** and **cell**

2. Little groups at the  $\Gamma$  point of the considered structures have a high symmetry preserving non-Abelian structure of rotations[147] and leading to degenerate irreducible representations, manifestations of which we observe as degenerate occupancies. Qualitatively, the frontier SA-NOs are very different from the ones expected from GK rules. First, SA-NO # 1 in **cell 1** (Fig 2) has large contributions from  $s$ -orbitals on oxygen, but the contribution from the  $p$ -orbitals is zero. While the Kanamori's paper [144] has a remark that  $s$ -orbitals do not violate the symmetry arguments leading to ferromagnetic interactions between nearest neighbors if the overlap between  $s$ - and  $d$ -orbitals is zero, they are not considered in the follow-up publications. The  $s$ - and  $d$ -orbitals composing SA-NO # 1 have a non-zero overlap, which makes the analysis non-trivial. The  $d$ -orbitals from the SA-NOs form symmetric and antisymmetric combinations. The net sum of occupations of the corresponding symmetric and antisymmetric SA-NOs occupations is close to 2, meaning that the electrons partly transfer from the antisymmetric SA-NOs (occupations are slightly smaller than 1) to the symmetric ones (occupations are slightly larger than 1), leading to magnetic interactions, since due to the Pauli repulsion such a redistribution of electrons with the same spin in the ferromagnetic solutions cannot happen.

SA-NOs # 1 and # 2 in **cell 2** (Fig. 3) have contributions from  $p$ -orbitals, but their orientation does not coincide with the  $d$ -orbitals, which becomes especially clear if the translation to the nearest-neighbors is applied (Fig. S1 in SI). This misalignment, resulting only in partial antibonding interactions, is also a deviation from the GK rules. In **cell 2**, SA-NOs # 1 and # 2 (partly antibonding orbitals) are partly depopulated; SA-NOs # 3 and # 4 (non-bonding orbitals) are partly populated, while the net sum of occupations between the corresponding symmetric and antisymmetric combinations is again close to 2. The occupancies of the corresponding bonding/antibonding SA-NOs explain the origin of partial charge transfer from the oxygen to the nickel atom.

#### D. Natural orbitals at other k-points

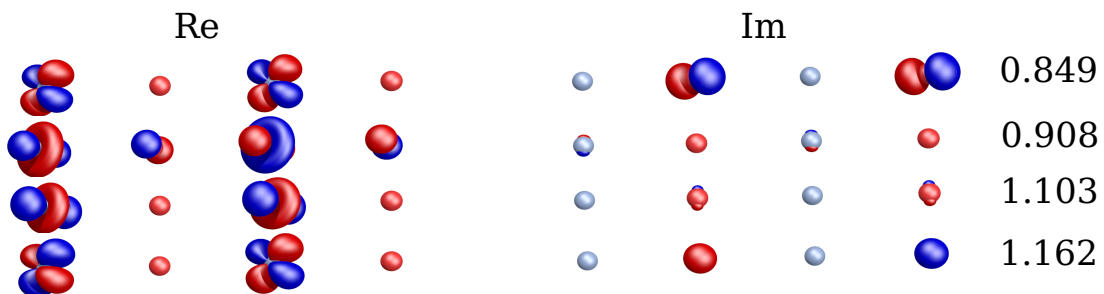


FIG. 4: SA-NOs and their occupancies computed from the broken-symmetry solutions at  $\vec{k} = (0.3986, 0.080, -0.8770)$  of NiO in **cell 2** within GW ( $\vec{k}$  is written in the absolute notation). Both real (left) and imaginary (right) parts of the SA-NOs are visualized.

Characters and occupations of SA-NOs depend strongly on momentum, which is again a violation of the prediction of the GK rules. Fig. 4 shows the frontier SA-NOs of NiO at one selected momentum point, where  $s$ -orbitals contribute to the imaginary part of the SA-NO. Due to a mixed character, interpretation of such orbitals in terms of bonding and antibonding orbitals is less straightforward. Nonetheless, even in this case the net sum

of occupancies for the corresponding mixed bonding/antibonding pairs of SA-NOs is close to 2. This remains true for other k-points. Fig. 5 shows occupancies of SA-NOs along

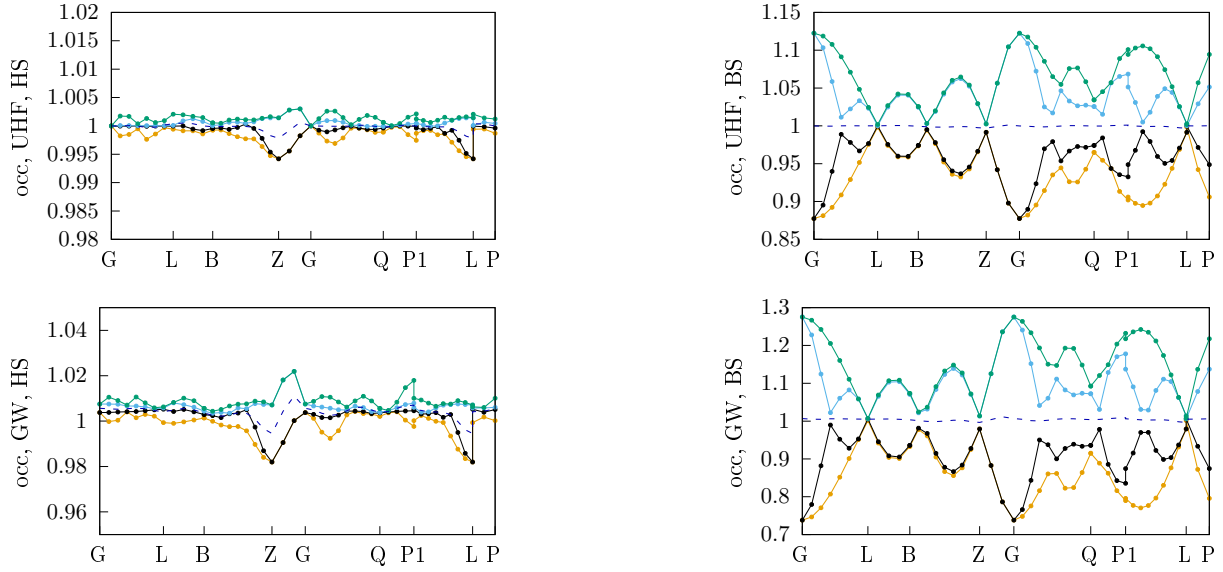


FIG. 5: Occupation numbers of the frontier SA-NOs for the k-points along the interpolated path for NiO in **cell 2** evaluated with UHF (top) and GW (down) with  $5 \times 5 \times 5$  grid for HS (left) and BS (right) solutions. The dashed blue line is the average of the occupancies of all 4 frontier SA-NOs at each k-point.

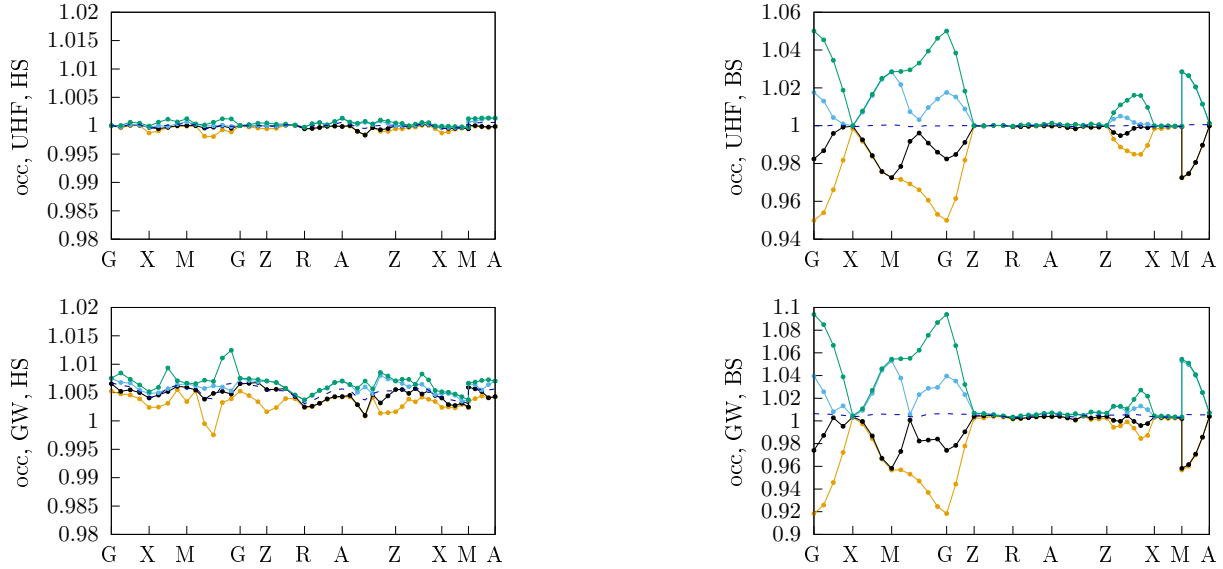


FIG. 6: Occupation numbers of the frontier SA-NOs for the k-points along the interpolated path for NiO in **cell 1** evaluated with UHF (top) and GW (down) with  $5 \times 5 \times 5$  grid for HS (left) and BS (right) solutions. The dashed blue line is the average of the occupancies of all 4 frontier SA-NOs at each k-point.

the Wannier interpolation path (k-path) in rhombohedral (type 1) **cell 2**. The SA-NO occupancies of the HS solution along the k-path are very flat and close to 1, meaning that the structure of the ferromagnetic solution is similar across different k-points (but the underlying composition of SA-NOs, of course, depends on momentum). The SA-NO occupancies of the BS solution show deviations from 1. Interestingly, these occupation deviations are almost perfectly symmetric with respect to the average occupation of these SA-NOs, which is almost a constant close to 1 along the entire k-path. This behavior is preserved when electron correlation is included by means of GW, implying that the main contributions to the differences between the solutions come from only these 4 frontier SA-NOs at each k-point. These general observations are also true for the occupancies of frontier SA-NOs at **cell 1** (Fig. 6), but the deviations from 1 are much smaller. All these patterns of occupation numbers along the corresponding *k*-paths are also preserved for CoO and FeO with 6 and 8 open-shell frontier SA-NOs, respectively, shown in Figs. S4, S5, S10, and S11 in SI.

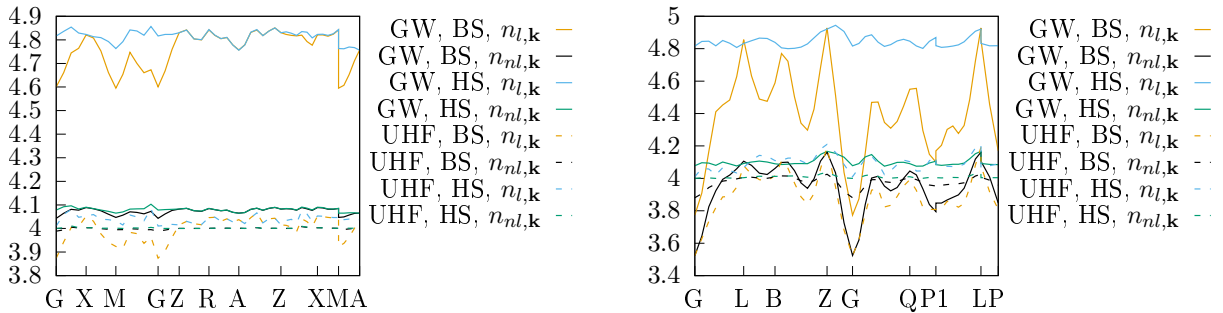


FIG. 7: Effective numbers of open-shell electrons for the UHF (dashed lines) and GW (solid lines) solutions in **cell 1** (left) and **cell 2** (right).

Fig. 7 shows the effective number of open-shell electrons of NiO along the interpolation k-path in both cells. For UHF,  $n_{l,\mathbf{k}}$  and  $n_{nl,\mathbf{k}}$  agree well and give an estimate close to 4. The nonlinear index,  $n_{nl,\mathbf{k}}$ , shows smaller deviations from 4 along the k-path. The difference between the indices increases when GW dynamic correlation is included since  $n_{l,\mathbf{k}}$  is more susceptible to a large number of small occupancies due to the presence of dynamic correlation. These observations are fully consistent with  $n_l$  and  $n_{nl}$  behavior for molecules[100]. In **cell 2**,  $n_{nl,\mathbf{k}}$  drops at a  $\Gamma$  point to a minimum along the k-path; there are also additional local minima. All these minima correspond to extremal differences in occupancies in Fig. 5. In **cell 1**,  $n_{nl,\mathbf{k}}$  is almost flat, while  $n_{l,\mathbf{k}}$  is sensitive enough to recognize smaller differences in occupancies in Fig. 6. Nonetheless, we notice that simple occupancies of the frontier SA-NOs are much easier to interpret than rather sophisticated indices  $n_{l,\mathbf{k}}$  and  $n_{nl,\mathbf{k}}$ .

Figs. 8 and 9 show squares of AO coefficients in BS UHF and GW SA-NOs in **cell 2** for NiO. While the character of the frontier SA-NOs change significantly along the k-path, only  $3d_{z^2}$  and  $3d_{x^2-y^2}$  AOs on nickel contribute in a chosen coordinate system, while the weights of other d-orbitals are negligible. Contributions from the oxygen orbitals also vary along the k-path, violating GK rules. All the  $2p$  orbitals contribute at different k-points. The contribution of the oxygen  $2s$  orbitals is very significant (highlighted by the blue fill) and is comparable with the  $2p$  orbitals, which is also not expected from the GK rules. The inclusion of electron correlation with GW does not change the picture qualitatively, but the weights of all contributions from oxygen increase, while the weights from nickel *d*-orbitals decrease.

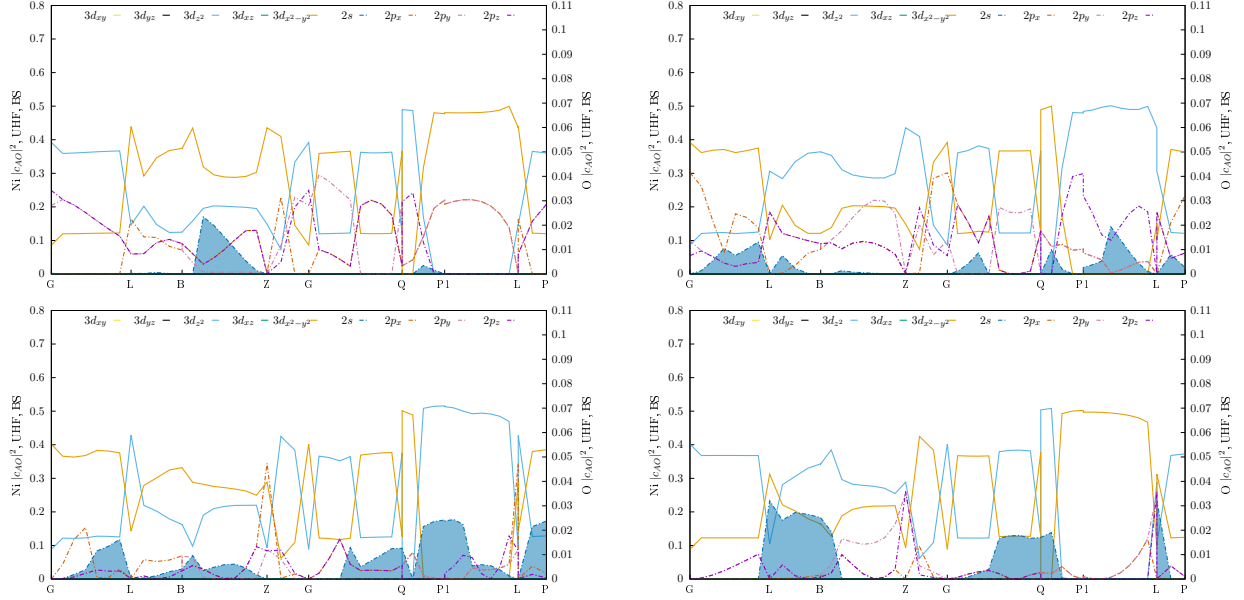


FIG. 8: Squared absolute values of atomic contributions to the UHF frontier SA-NOs along Wannier interpolation path in **cell 2**. The contributions of  $3d$  AOs from the first nickel atom in the cell are shown by solid curves; the contributions of  $2s$  and  $2p$  AOs from the first oxygen atom are shown in dashed-dotted lines. The areas below  $2s$  curves are filled to highlight contributions from the  $s$ -orbitals.

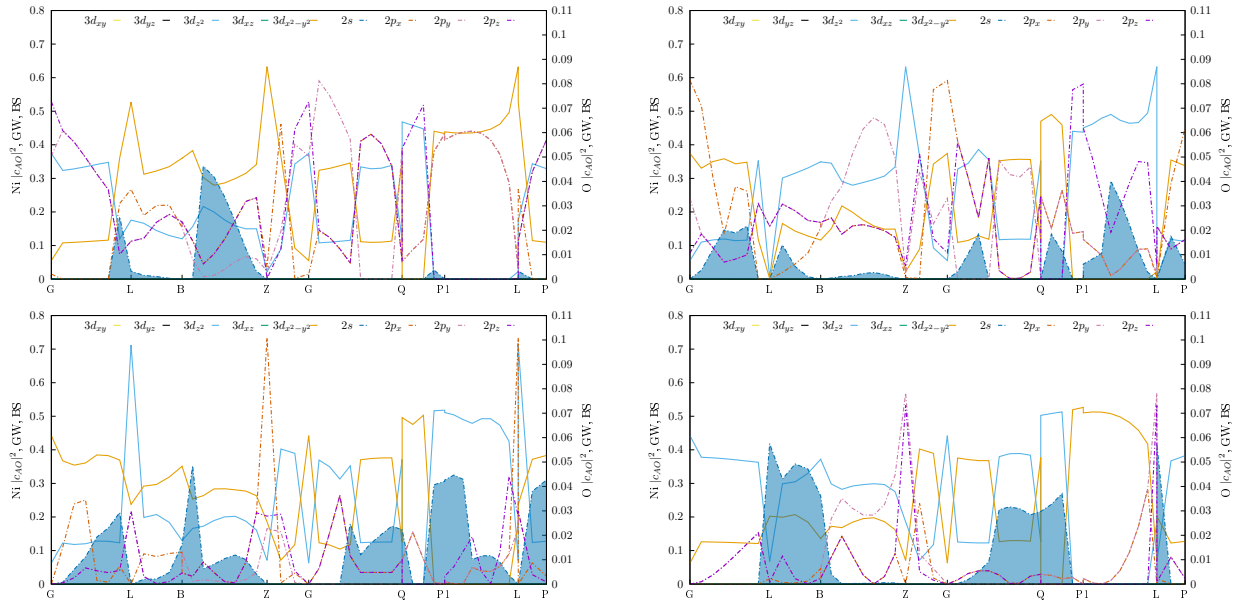


FIG. 9: Squared absolute values of atomic contributions to the GW frontier SA-NOs along Wannier interpolation path in **cell 2**. The contributions of  $3d$  AOs from the first nickel atom in the cell are shown by solid curves; the contributions of  $2s$  and  $2p$  AOs from the first oxygen atom are shown in dashed-dotted lines. The areas below  $2s$  curves are filled to highlight contributions from the  $s$ -orbitals.

All of these observations are also true for the BS solution in **cell 1** (Figs. S2 and S3 in SI) along the corresponding k-path, where the weights of the  $2s$  orbital on oxygen in SA-NOs are even bigger than in **cell 2**. Figs. S6, S7, S8, and S9 in SI show the AO composition of the frontier SA-NOs for CoO in **cell 2** and **cell 1**. Generally, all five  $d$ -orbitals contribute to SA-NOs, but in **cell 2** the most depopulated and the most populated frontier SA-NO have characters, similar to the ones for NiO. This suggests that the mechanism of superexchange leading to  $J_2$  is similar in both compounds. The character of SA-NOs in **cell 1** does not show this similarity, and the character of the most depopulated and populated frontier SA-NOs is mainly determined by cobalt  $d_{xy}$ ,  $d_{yz}$ , and  $d_{x^2-y^2}$  AOs, indicating a different mechanism leading to  $J_1$ . Figs. S12, S13, S14, and S15 in SI show the AO composition of the frontier SA-NOs for FeO in **cell 2** and **cell 1**. Again, all five  $d$ -orbitals contribute to SA-NOs, but in **cell 2** the most depopulated and the most populated frontier SA-NO have a character, mostly similar to the ones for NiO and CoO (there is a local intrusion of  $d_{yz}$  and  $d_{xy}$  AOs near  $B$  and  $Q$  points). In **cell 1**, the most depopulated and the most populated frontier SA-NOs are strongly dominated by  $d_{yz}$  and are different from both NiO and CoO. In all the cells for all the considered compounds, GW preserves the overall character of the frontier SA-NOs, but increases the weights of the  $s$ - and  $p$ -orbitals on oxygen and decreases the weights of the  $d$ -orbitals on metal atoms.

### E. Two-particle correlators

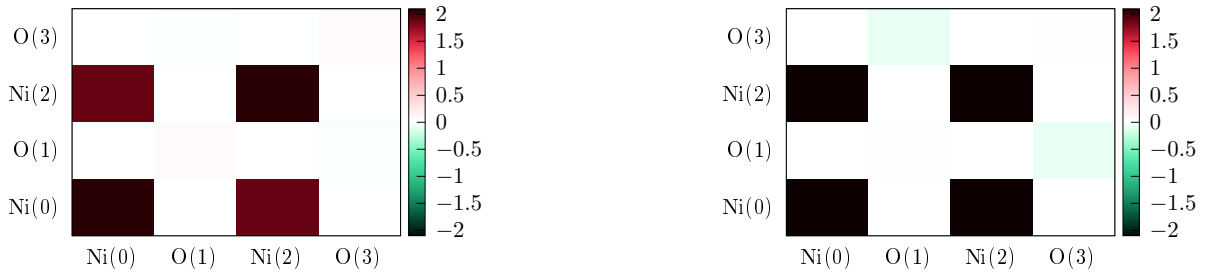


FIG. 10: Difference of  $NN_{AB}^{k=0}$  between the HS and BS solutions, computed for the NiO **cell 2** with UHF (left) and GW (right) with  $5 \times 5 \times 5$  grid.

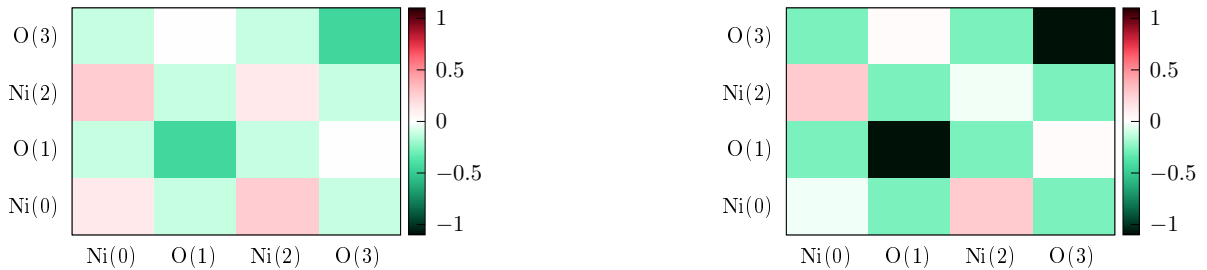


FIG. 11: Difference of  $NN_{AB}$  between the HS and BS solutions, computed for the NiO **cell 2** with UHF (left) and GW (right) with  $5 \times 5 \times 5$  grid.

The local two-particle correlators are shown in Figs. 10 and 11. The  $NN_{AB}^{k=0}$  correlators show a significant difference in charge correlators on nickel centers, while the correlator difference between nickel and oxygen is surprisingly small. A possible cause behind this behaviour is due to smaller contributions from a single oxygen AOs to SA-NO #1 and #2 in Fig. 3  $\sum_i c_{2p_i}^2 = 0.062$  (UHF) and  $\sum_i c_{2p_i}^2 = 0.125$  (GW) than from a single nickel AOs  $\sum_j c_{3d_j}^2 = 0.479$  (UHF) and  $\sum_j c_{3d_j}^2 = 0.431$  (GW), where we do not include weights of polarization functions for simplicity. The  $NN_{AB}$  averages across all  $k$ -points, reducing the difference for Ni–Ni correlators and increasing the difference for the Ni–O correlators. Since the  $NN_{AB}$  corresponds to a real-space charge correlator in localized orbitals, it clearly indicates that locally charge transfer from oxygen to nickel is rather substantial.

### F. Role of electron correlation

A renormalized interaction  $W$ , captured by GW, satisfies a Dyson-like equation. Because of this renormalization,  $W$  describes screening that reduces the strength of the Coulomb interaction. Therefore, one would expect that the weight of charge-transfer contributions would become more prominent. In particular, one can expect an enhancement of charge transfer between oxygen and metal centers. This leads to an increase of AO coefficients of  $s$ - and  $p$ -orbitals and decrease of the coefficients of  $d$ -orbitals, which we observe for all SA-NOs for all the compounds in all the cells. Screening also leads to an increase of occupancy deviation from 1 for the broken-symmetry solutions for all the compounds and for all the cells, while preserving the overall character of the SA-NOs. At the two-particle level, screening also enhances the differences in local charge correlators, which also confirms the increase of the charge-transfer character.

## IV. CONCLUSIONS AND IMPLICATIONS FOR THE FUTURE

We generalized the concepts of natural orbitals and spin-averaged natural orbitals. We also generalized the  $n_l$  and  $n_{nl}$  indices—the effective numbers of open-shell electrons—for solids. Using these concepts, we analyzed electronic structure of cubic rock-salt transition-metal oxides: NiO, CoO, FeO. Our findings disagree with the qualitative Goodenough–Kanamori rules, formulated on semiempirical grounds almost half a century ago. Only the frontier SA-NOs are responsible for magnetic physics. Specifically, a complicated momentum behavior of the SA-NO occupation numbers for the broken-symmetry solutions is in a disagreement with the predictions deduced from Goodenough–Kanamori rules. All the frontier SA-NOs of the broken-symmetry solutions form pairs, net occupancy of which is close to 2; occupancies of all the frontier SA-NOs of the high-spin solutions is close to 1. This gives a clear picture of the effective exchange coupling, related to a chemical concept of multielectron multicenter bonding. The character of the frontier SA-NOs of the broken-symmetry solutions change significantly along the interpolated  $k$ -paths in the corresponding unit cells. This is also in a disagreement with Goodenough–Kanamori rules. In particular, we found that  $p$ -orbitals on oxygen are as important as  $s$ -orbitals, which have not been considered before in simplistic models. This finding not only affects the qualitative picture of magnetic interactions, but also indicates that  $s$ -orbitals must be included in the active spaces used in embedded methods, such as a self-energy embedding theory[109, 148–155]. The character and physics of the SA-NOs in our calculations are qualitatively different from the NOs of

the localized clusters, considered in Ref.156. The effective number of open-shell electrons, captured by  $n_{l,\mathbf{k}}$  and  $n_{nl,\mathbf{k}}$  indices, show how dynamic correlation changes the occupation numbers.

We found that in the considered insulators the analysis of the frontier SA-NOs provides more insights into the mechanism of effective exchange couplings. We also generalized local two-particle charge correlators and used them to confirm the changes in charge-transfer character of the solutions. Inclusion of correlation through screened interaction  $W$  enhanced the charge-transfer character of the solutions, which is seen in SA-NO occupancies, SA-NO compositions, and two-particle correlators. We and others previously observed the enhancement of charge-transfer character by dynamic correlation in multiple bridged molecular transition-metal complexes[26, 95, 96]; however, explanations of this phenomenon in the multireference wave-function methods was lacking, which we now can attribute to the presence of screening. Broken-symmetry fully self-consistent GW gives much more accurate values of effective exchange couplings. This analysis implies, for example, that a complete-active-space self-consistent field method should give poor estimates of the effective exchange couplings due to insufficient screening, explaining why only very large active spaces are sufficient for reasonable estimates, which is often observed in practice. The analysis above also has implications for DFT. While the majority of DFT functionals give unsatisfactory effective exchange constants for transition-metal oxides, the best-performing functional from Ref[142] is HSE. This functional is based on Coulomb attenuation of PBE in the long-range part with some empirical mixture of HF exchange and PBE in the short-range part[157]. The Coulomb attenuation mimics the effects of screening, which is the most important part of the magnetic physics in these systems, explaining a good performance of this functional in comparison to other functionals without screening. Due to this theoretical justification, we recommend to start search of DFT functional for evaluation of effective exchange couplings from the Coulomb-attenuated family of methods. Finally, since broken-symmetry fully self-consistent GW gives results comparable with multireference CI[26] and difference-dedicated CI[27], it is a good starting point for a perturbation theory based on renormalized interaction  $W$  and renormalized propagator  $G$  and included through a 3-point vertex function. We predict that such a screened perturbation theory converges rapidly and gives highly accurate effective exchange couplings, which we will pursue in the near future.

### Acknowledgments

P.P. and D.Z. acknowledge support from were supported by the Simons Foundation via the Simons Collaboration on the Many-Electron problem. We thank Dr. Gaurav Harsha for providing a band plotting script, which we modified to produce the plots along the interpolated  $k$ -paths.

## Supplementary Material

NiO natural orbitals; atomic contributions to the frontier SA-NOs for NiO, CoO, and FeO; occupancies of the frontier SA-NOs for CoO and FeO.

---

- [1] J. Miralles, O. Castell, R. Caballol, and J.-P. Malrieu, Specific CI calculation of energy differences: Transition energies and bond energies, *Chem. Phys.* **172**, 33 (1993).
- [2] A. E. Rask and P. M. Zimmerman, Toward full configuration interaction for transition-metal complexes, *J. Phys. Chem. A* **125**, 1598 (2021).
- [3] K. Andersson, P.-Å. Malmqvist, B. O. Roos, A.J. Sadlej, and K. Wolinski, 2nd order perturbation theory with a CASSCF reference function, *J. Phys. Chem.* **94**, 5483 (1990).
- [4] Celestino Angeli, Renzo Cimiraglia, and Jean-Paul Malrieu, n-electron valence state perturbation theory: A spinless formulation and an efficient implementation of the strongly contracted and of the partially contracted variants, *J. Chem. Phys.* **117**, 9138 (2002).
- [5] C. Angeli, R. Cimiraglia, S. Evangelisti, T. Leininger, and J.-P. Malrieu, Introduction of n-electron valence states for multireference perturbation theory, *J. Chem. Phys.* **114**, 10252 (2001).
- [6] D. Casanova and A. I. Krylov, Spin-flip methods in quantum chemistry, *Phys. Chem. Chem. Phys.* **22**, 4326 (2020).
- [7] Y. Shao, M. Head-Gordon, and A. I. Krylov, The spin-flip approach within time-dependent density functional theory: Theory and applications to diradicals, *J. Chem. Phys.* **118**, 4807 (2003).
- [8] Y. A. Bernard, Y. Shao, and A. I. Krylov, General formulation of spin-flip time-dependent density functional theory using non-collinear kernels: Theory, implementation, and benchmarks, *J. Chem. Phys.* **136**, 204103 (2012).
- [9] F. Wang and T. Ziegler, Time-dependent density functional theory based on a noncollinear formulation of the exchange-correlation potential, *J. Chem. Phys.* **121**, 12191 (2004).
- [10] H. R. Zhekova, M. Seth, and T. Ziegler, Calculation of the exchange coupling constants of copper binuclear systems based on spin-flip constricted variational density functional theory, *J. Chem. Phys.* **135**, 184105 (2011).
- [11] H. R. Zhekova, M. Seth, and T. Ziegler, Calculation of the exchange coupling constants of

- copper binuclear systems based on spin-flip constricted variational density functional theory, *J. Chem. Phys.* **135**, 184105 (2012).
- [12] I. Seidu, H. R. Zhekova, M. Seth, and T. Ziegler, Calculation of exchange coupling constants in triply-bridged dinuclear Cu(II) compounds based on spin-flip constricted variational density functional theory, *J. Phys. Chem. A* **116**, 2268 (2012).
- [13] H. R. Zhekova, M. Seth, and T. Ziegler, Introduction of a new theory for the calculation of magnetic coupling based on spin flip constricted variational density functional theory. Application to trinuclear copper complexes which model the native intermediate in multicopper oxidases, *J. Chem. Theory Comput.* **7**, 1858–1866 (2011).
- [14] Z. D. Li and W. J. Liu, Spin-adapted open-shell random phase approximation and time-dependent density functional theory. I. Theory, *J. Chem. Phys.* **133**, 064106 (2010).
- [15] Z. D. Li, W. J. Liu, Y. Zhang, and B. B. Suo, Spin-adapted open-shell time-dependent density functional theory. II. Theory and pilot application, *J. Chem. Phys.* **134**, 134101 (2011).
- [16] R. Valero, F. Illas, and D. G. Truhlar, Magnetic coupling in transition-metal binuclear complexes by spin-flip time-dependent density functional theory, *J. Chem. Theory Comput.* **7**, 3523 (2011).
- [17] N. Orms and A. I. Krylov, Singlet-triplet energy gaps and the degree of diradical character in binuclear copper molecular magnets characterized by spin-flip density functional theory, *Phys. Chem. Chem. Phys.* **20**, 13127 (2018).
- [18] S. Kotaru, S. Kähler, M. Alessio, and A. I. Krylov, Magnetic exchange interactions in binuclear and tetranuclear iron(III) complexes described by spin-flip DFT and Heisenberg effective Hamiltonians, *J. Comput. Chem.* **n/a**.
- [19] A. I. Krylov, Size-consistent wave functions for bond-breaking: The equation-of-motion spin-flip model, *Chem. Phys. Lett.* **338**, 375 (2001).
- [20] D. Casanova, L. V. Slipchenko, A. I. Krylov, and M. Head-Gordon, Double spin-flip approach within equation-of-motion coupled cluster and configuration interaction formalisms: Theory, implementation and examples, *J. Chem. Phys.* **130**, 044103 (2009).
- [21] G. P. Paran, C. Utku, and T.-C. Jagau, A spin-flip variant of the second-order approximate coupled-cluster singles and doubles method, *Phys. Chem. Chem. Phys.* **24**, 27146 (2022).
- [22] Y. Takahara, K. Yamaguchi, and T. Fueno, Potential energy curves for transition metal dimers and complexes calculated by the approximately projected unrestricted Hartree–Fock

- and Møller–Plesset perturbation (APUMP) methods, *Chem. Phys. Lett.* **158**, 95 (1989).
- [23] T. Saito, A. Ito, T. Watanabe, T. Kawakami, M. Okumura, and K. Yamaguchi, Performance of the coupled cluster and DFT methods for through-space magnetic interactions of nitroxide dimer, *Chem. Phys. Lett.* **542**, 19 (2012).
- [24] H. Schurkus, D.-T. Chen, H.-P. Cheng, G. Chan, and J. Stanton, Theoretical prediction of magnetic exchange coupling constants from broken-symmetry coupled cluster calculations, *J. Chem. Phys.* **152**, 234115 (2020).
- [25] A. Mansikkamäki, Z. Huang, N. Iwahara, and L. F. Chibotaru, Broken symmetry  $G_0W_0$  approach for the evaluation of exchange coupling constants, <https://arxiv.org/abs/2003.06334> (2020).
- [26] P. Pokhilko and D. Zgid, Interpretation of multiple solutions in fully iterative GF2 and GW schemes using local analysis of two-particle density matrices, *J. Chem. Phys.* **155**, 024101 (2021).
- [27] P. Pokhilko and D. Zgid, Broken-symmetry self-consistent GW approach: Degree of spin contamination and evaluation of effective exchange couplings in solid antiferromagnets, *J. Chem. Phys.* **157**, 144101 (2022).
- [28] A.I. Liechtenstein, M.I. Katsnelson, V.P. Antropov, and V.A. Gubanov, Local spin density functional approach to the theory of exchange interactions in ferromagnetic metals and alloys, *J. Magn. Magn. Mater.* **67**, 65 (1987).
- [29] L. E. Aebersold, A. R. Hale, G. Christou, and J. E. Peralta, Validation of the Green’s function approximation for the calculation of magnetic exchange couplings, *J. Phys. Chem. A* **126**, 6790 (2022).
- [30] I. de P. R. Moreira, F. Illas, and R. L. Martin, Effect of Fock exchange on the electronic structure and magnetic coupling in NiO, *Phys. Rev. B* **65**, 155102 (2002).
- [31] C. de Graaf, C. Sousa, I. de P. R. Moreira, and F. Illas, Multiconfigurational perturbation theory: An efficient tool to predict magnetic coupling parameters in biradicals, molecular complexes, and ionic insulators, *J. Phys. Chem. A* **105**, 11371 (2001).
- [32] P. Pokhilko, D. S. Bezrukov, and A. I. Krylov, Is solid copper oxalate a spin chain or a mixture of entangled spin pairs?, *J. Phys. Chem. C* **125**, 7502 (2021).
- [33] L. Noodleman, Valence bond description of antiferromagnetic coupling in transition metal dimers, *J. Chem. Phys.* **74**, 5737 (1981).

- [34] K. Yamaguchi, Y. Takahara, and T. Fueno, Ab-initio molecular orbital studies of structure and reactivity of transition metal-oxo compounds, in *Applied quantum chemistry*, pages 155–184. Springer, 1986.
- [35] G. David, N. Ferré, G. Trinquier, and J.-P. Malrieu, Improved evaluation of spin-polarization energy contributions using broken-symmetry calculations, *J. Chem. Phys.* **153**, 054120 (2020).
- [36] G. David, G. Trinquier, and J.-P. Malrieu, Consistent spin decontamination of broken-symmetry calculations of diradicals, *J. Chem. Phys.* **153**, 194107 (2020).
- [37] J. Gräfenstein and D. Cremer, On the diagnostic value of  $\langle \hat{S}^2 \rangle$  in Kohn–Sham density functional theory, *Mol. Phys.* **99**, 981 (2001).
- [38] A. J. Cohen, D. J. Tozer, and N. C. Handy, Evaluation of  $\langle S^2 \rangle$  in density functional theory, *J. Chem. Phys.* **126**, 214104 (2007).
- [39] J. Wang, A. D. Becke, and V. H. Smith, Evaluation of  $\langle S^2 \rangle$  in restricted, unrestricted Hartree–Fock, and density functional based theories, *J. Chem. Phys.* **102**, 3477 (1995).
- [40] K. Tada, S. Yamanaka, T. Kawakami, Y. Kitagawa, M. Okumura, K. Yamaguchi, and S. Tanaka, Estimation of spin contamination errors in DFT/plane-wave calculations of solid materials using approximate spin projection scheme, *Chem. Phys. Lett.* **765**, 138291 (2021).
- [41] G. D. Mahan, *Many-Particle Physics*, Physics of Solids and Liquids. Springer, 2000.
- [42] J. W. Negele and H. Orland, *Quantum many-particle systems*. CRC Press, 2018.
- [43] R. M. Martin, L. Reining, and D. M. Ceperley, *Interacting electrons*. Cambridge University Press, 2016.
- [44] C.-O. Almbladh, On the theory of photoemission, *Phys. Scr.* **32**, 341 (1985).
- [45] W. Bardyszewski and L. Hedin, A new approach to the theory of photoemission from solids, *Phys. Scr.* **32**, 439 (1985).
- [46] T. Fujikawa and K. Niki, *Theory of Photoelectron Spectroscopy*, volume 209, pages 285–301. Springer Japan, Tokyo, 2015.
- [47] L. P. Kadanoff and P. C. Martin, Theory of many-particle systems. II. Superconductivity, *Phys. Rev.* **124**, 670 (1961).
- [48] J. M. Luttinger and J. C. Ward, Ground-state energy of a many-fermion system. II, *Phys. Rev.* **118**, 1417 (1960).
- [49] G. Baym and L. P. Kadanoff, Conservation laws and correlation functions, *Phys. Rev.* **124**, 287 (1961).

- [50] G. Baym, Self-consistent approximations in many-body systems, *Phys. Rev.* **127**, 1391 (1962).
- [51] P. Pokhilko, S. Isakov, C.-N. Yeh, and D. Zgid, Evaluation of two-particle properties within finite-temperature self-consistent one-particle Green's function methods: Theory and application to GW and GF2, *J. Chem. Phys.* **155**, 024119 (2021).
- [52] J. des Cloizeaux, Extension d'une formule de lagrange à des problèmes de valeurs propres, *Nucl. Phys.* **20**, 321 (1960).
- [53] C. Bloch, Sur la théorie des perturbations des états liés, *Nucl. Phys.* **6**, 329 (1958).
- [54] S. Ôkubo, Diagonalization of Hamiltonian and Tamm-Dancoff equation, *Prog. Theor. Phys.* **12**, 603 (1954).
- [55] P. Durand, Direct determination of effective hamiltonians by wave-operator methods. I. General formalism, *Phys. Rev. A* **28**, 3184 (1983).
- [56] C. E. Soliveres, An effective hamiltonian and time-independent perturbation theory, *J. Phys. C: Solid State Phys.* **2**, 2161 (1969).
- [57] C. J. Calzado, J. Cabrero, J. P. Malrieu, and R. Caballol, Analysis of the magnetic coupling in binuclear complexes. II. Derivation of valence effective hamiltonians from ab initio CI and DFT calculations, *J. Chem. Phys.* **116**, 3985 (2002).
- [58] J. P. Malrieu, R. Caballol, C. J. Calzado, C. de Graaf, and N. Guihéry, Magnetic interactions in molecules and highly correlated materials: Physical content, analytical derivation, and rigorous extraction of magnetic Hamiltonians, *Chem. Rev.* **114**, 429 (2013).
- [59] A. A. Buchachenko, G. Chałasiński, and M. M. Szcześniak, Electronic structure and spin coupling of the manganese dimer: The state of the art of ab initio approach, *J. Chem. Phys.* **132**, 024312 (2010).
- [60] N. J. Mayhall and M. Head-Gordon, Computational quantum chemistry for single Heisenberg spin couplings made simple: Just one spin flip required, *J. Chem. Phys.* **141**, 134111 (2014).
- [61] N. J. Mayhall and M. Head-Gordon, Computational quantum chemistry for multiple-site Heisenberg spin couplings made simple: Still only one spin-flip required, *J. Phys. Chem. Lett.* **6**, 1982 (2015).
- [62] P. Pokhilko and A. I. Krylov, Effective Hamiltonians derived from equation-of-motion coupled-cluster wave-functions: Theory and application to the Hubbard and Heisenberg Hamiltonians, *J. Chem. Phys.* **152**, 094108 (2020).

- [63] P. Pokhilko and D. Zgid, Evaluation of Neel temperatures from fully self-consistent broken-symmetry GW and high-temperature expansion: application to cubic transition-metal oxides, page <https://arxiv.org/abs/2209.14904> (2022).
- [64] H. A. Kramers, L'interaction entre les atomes magnétogènes dans un cristal paramagnétique, *Physica* **1**, 182 (1934).
- [65] P. W. Anderson, Antiferromagnetism. theory of superexchange interaction, *Phys. Rev.* **79**, 350 (1950).
- [66] P. W. Anderson, Theory of magnetic exchange interactions:exchange in insulators and semiconductors, volume 14 of *Solid State Phys.*, pages 99–214. Academic Press, 1963.
- [67] M. V. Eremin and Yu. V. Rakitin, On kinetic exchange theory, *Phys. Stat. Sol. (b)* **97**, 51 (1980).
- [68] E. Coulaud, N. Guihéry, J.-P. Malrieu, D. Hagebaum-Reignier, D. Siri, and N. Ferré, Analysis of the physical contributions to magnetic couplings in broken symmetry density functional theory approach, *J. Chem. Phys.* **137**, 114106 (2012).
- [69] E. Coulaud, J.-P. Malrieu, N. Guihéry, and N. Ferré, Additive decomposition of the physical components of the magnetic coupling from broken symmetry density functional theory calculations, *J. Chem. Theory Comput.* **9**, 3429 (2013).
- [70] G. David, F. Wennmohs, F. Neese, and N. Ferré, Chemical tuning of magnetic exchange couplings using broken-symmetry density functional theory, *Inorg. Chem.* **57**, 12769 (2018).
- [71] G. David, N. Ferré, and B. Le Guennic, Consistent evaluation of magnetic exchange couplings in multicenter compounds in KS-DFT: The recomposition method, *J. Chem. Theory Comput.* **19**, 157 (2023).
- [72] In principle, one can merge momentum, spin, space coordinate, and time. For example, the corresponding multiindex is a convenient label for two-particle Green's functions. However, in this paper, we focus on analysis of one- and two-particle quantities at zero time slice, so for our purposes we keep the time label separately.
- [73] Note that other choices are possible as well with Green's functions, such as restricted ( $G_{\alpha\alpha} = G_{\beta\beta}$ ,  $G_{\alpha\beta} = G_{\beta\alpha} = 0$ ) and generalized ( $G_{\alpha\alpha}$ ,  $G_{\beta\beta}$ ,  $G_{\alpha\beta}$ ,  $G_{\beta\alpha}$  are non-zero and possibly different).
- [74] A. V. Luzanov, A. A. Sukhorukov, and V. E. Umanskii, Application of transition density matrix for analysis of excited states, *Theor. Exp. Chem.* **10**, 354 (1976), Russian original:

- Teor. Eksp. Khim., 10, 456 (1974).
- [75] A. V. Luzanov and V. F. Pedash, Interpretation of excited states using charge-transfer number, *Theor. Exp. Chem.* **15**, 338 (1979).
- [76] M. Head-Gordon, A. M. Grana, D. Maurice, and C. A. White, Analysis of electronic transitions as the difference of electron attachment and detachment densities, *J. Phys. Chem.* **99**, 14261 (1995).
- [77] R. L. Martin, Natural transition orbitals, *J. Phys. Chem. A* **118**, 4775 (2003).
- [78] A. V. Luzanov and O. A. Zhikol, Excited state structural analysis: TDDFT and related models, in *Practical aspects of computational chemistry I: An overview of the last two decades and current trends*, edited by J. Leszczynski and M.K. Shukla, pages 415–449. Springer, 2012.
- [79] F. Plasser, M. Wormit, and A. Dreuw, New tools for the systematic analysis and visualization of electronic excitations. I. formalism, *J. Chem. Phys.* **141**, 024106 (2014).
- [80] F. Plasser, S. A. B appler, M. Wormit, and A. Dreuw, New tools for the systematic analysis and visualization of electronic excitations. II. Applications, *J. Chem. Phys.* **141**, 024107 (2014).
- [81] S. A. Mewes, J.-M. Mewes, A. Dreuw, and F. Plasser, Excitons in poly(para phenylene vinylene): a quantum-chemical perspective based on high-level ab initio calculations, *Phys. Chem. Chem. Phys.* **18**, 2548 (2016).
- [82] K. D. Nanda and A. I. Krylov, Visualizing the contributions of virtual states to two-photon absorption cross-sections by natural transition orbitals of response transition density matrices, *J. Phys. Chem. Lett.* **8**, 3256 (2017).
- [83] W. Skomorowski and A. I. Krylov, Real and imaginary excitons: Making sense of resonance wavefunctions by using reduced state and transition density matrices, *J. Phys. Chem. Lett.* **9**, 4101 (2018).
- [84] S. Mewes, F. Plasser, A. I. Krylov, and A. Dreuw, Benchmarking excited-state calculations using exciton properties, *J. Chem. Theory Comput.* **14**, 710 (2018).
- [85] S. A. Mewes and A. Dreuw, Density-based descriptors and exciton analyses for visualizing and understanding the electronic structure of excited states, *Phys. Chem. Chem. Phys.* **21**, 2843 (2019).
- [86] P. Pokhilko and A. I. Krylov, Quantitative El-Sayed rules for many-body wavefunctions from spinless transition density matrices, *J. Phys. Chem. Lett.* **10**, 4857 (2019).

- [87] A. I. Krylov, From orbitals to observables and back, *J. Chem. Phys.* **153**, 080901 (2020).
- [88] F. Plasser, Visualisation of electronic excited-state correlation in real space, *ChemPhotoChem* **3**, 702 (2019).
- [89] K. D. Nanda and A. I. Krylov, A simple molecular orbital picture of RIXS distilled from many-body damped response theory, *J. Chem. Phys.* **152**, 244118 (2020).
- [90] M. de Wergifosse and S. Grimme, A unified strategy for the chemically intuitive interpretation of molecular optical response properties, *J. Chem. Theory Comput.* **16**, 7709 (2020).
- [91] K. D. Nanda and A. I. Krylov, The orbital picture of the first dipole hyperpolarizability from many-body response theory, *J. Chem. Phys.* **154**, 184109 (2021).
- [92] O. Kahn, *Molecular Magnetism*. VCH, 1993.
- [93] T. Soda, Y. Kitagawa, T. Onishi, Y. Takano, Y. Shigeta, H. Nagao, Y. Yoshioka, and K. Yamaguchi, Ab initio computations of effective exchange integrals for H–H, H–He–H and Mn<sub>2</sub>O<sub>2</sub> complex: comparison of broken-symmetry approaches, *Chem. Phys. Lett.* **319**, 223 (2000).
- [94] J. Cabrero, C. J. Calzado, D. Maynau, R. Caballol, and J. P. Malrieu, Metal–ligand delocalization in magnetic orbitals of binuclear complexes, *J. Phys. Chem. A* **106**, 8146 (2002).
- [95] T. V. Harris, Y. Kurashige, T. Yanai, and K. Morokuma, Ab initio density matrix renormalization group study of magnetic coupling in dinuclear iron and chromium complexes, *J. Chem. Phys.* **140**, 054303 (2014).
- [96] P. Sharma, D. G. Truhlar, and L. Gagliardi, Magnetic coupling in a tris-hydroxo-bridged chromium dimer occurs through ligand mediated superexchange in conjunction with through-space coupling, *J. Am. Chem. Soc.* **142**, 16644 (2020).
- [97] A. Grüneis, G. H. Booth, M. Marsman, J. Spencer, A. Alavi, and G. Kresse, Natural orbitals for wave function based correlated calculations using a plane wave basis set, *J. Chem. Theory Comput.* **7**, 2780 (2011).
- [98] N. H. March, G. G. N. Angilella, and R. Pucci, Natural orbitals in relation to quantum information theory: from model light atoms through to emergent metallic properties, *Int. J. Mod. Phys. B* **27**, 1330021 (2013).
- [99] K. Takatsuka, T. Fueno, and K. Yamaguchi, Distribution of odd electrons in ground-state molecules, *Theor. Chim. Acta* **48**, 175 (1978).
- [100] M. Head-Gordon, Characterizing unpaired electrons from the one-particle density matrix, *Chem. Phys. Lett.* **372**, 508 (2003).

- [101] L. Hedin, New method for calculating the one-particle Green's function with application to the electron-gas problem, *Phys. Rev.* **139**, A796 (1965).
- [102] W. E. Pickett and C. S. Wang, Local-density approximation for dynamical correlation corrections to single-particle excitations in insulators, *Phys. Rev. B* **30**, 4719 (1984).
- [103] M. S. Hybertsen and S. G. Louie, Electron correlation in semiconductors and insulators: Band gaps and quasiparticle energies, *Phys. Rev. B* **34**, 5390 (1986).
- [104] F. Aryasetiawan and O. Gunnarsson, The GW method, *Rep. Prog. Phys.* **61**, 237 (1998).
- [105] A. Stan, N. E. Dahlen, and R. van Leeuwen, Fully self-consistent GW calculations for atoms and molecules, *EPL* **76**, 298 (2006).
- [106] P. Koval, D. Foerster, and D. Sánchez-Portal, Fully self-consistent GW and quasiparticle self-consistent GW for molecules, *Phys. Rev. B* **89**, 155417 (2014).
- [107] A. Kutepov, Sergey Y. Savrasov, and G. Kotliar, Ground-state properties of simple elements from GW calculations, *Phys. Rev. B* **80**, 041103(R) (2009).
- [108] A. L. Kutepov, Self-consistent solution of Hedin's equations: Semiconductors and insulators, *Phys. Rev. B* **95**, 195120 (2017).
- [109] S. Isakov, C.-N. Yeh, E. Gull, and D. Zgid, Ab initio self-energy embedding for the photoemission spectra of NiO and MnO, *Phys. Rev. B* **102**, 085105 (2020).
- [110] C.-N. Yeh, S. Isakov, D. Zgid, and E. Gull, Fully self-consistent finite-temperature GW in Gaussian Bloch orbitals for solids, *Phys. Rev. B* **106**, 235104 (2022).
- [111] R. Kubo, Generalized cumulant expansion method, *J. Phys. Soc. Jap.* **17**, 1100 (1962).
- [112] K. Ruedenberg, The physical nature of the chemical bond, *Rev. Mod. Phys.* **34**, 326 (1962).
- [113] M. S. de Giambiagi, M. Giambiagi, and F. E. Jorge, Bond index: relation to second-order density matrix and charge fluctuations, *Theor. Chim. Acta* **68**, 337 (1985).
- [114] A. Torre, L. Lain, R. Bochicchio, and R. Ponec, Topological population analysis from higher order densities II. The correlated case, *J. Math. Chem.* **32**, 241 (2002).
- [115] A. Torre, L. Lain, and R. Bochicchio, Bond orders and their relationships with cumulant and unpaired electron densities, *J. Phys. Chem. A* **107**, 127 (2003).
- [116] T. Yamasaki and W. A. Goddard, Correlation analysis of chemical bonds, *J. Phys. Chem. A* **102**, 2919 (1998).
- [117] A. V. Luzanov and O. V. Prezhdo, Irreducible charge density matrices for analysis of many-electron wave functions, *Int. J. Quant. Chem.* **102**, 582 (2005).

- [118] I. Mayer, Bond order and valence indices: A personal account, *J. Comput. Chem.* **28**, 204 (2007).
- [119] A. E. Clark and E. R. Davidson, Local spin, *J. Chem. Phys.* **115**, 7382 (2001).
- [120] E. R. Davidson and A. E. Clark, Local spin II, *Mol. Phys.* **100**, 373 (2002).
- [121] E. R. Davidson and A. E. Clark, Model molecular magnets, *J. Phys. Chem. A* **106**, 7456 (2002).
- [122] C. Herrmann, M. Reiher, and B. A. Hess, Comparative analysis of local spin definitions, *J. Chem. Phys.* **122**, 034102 (2005).
- [123] A. V. Luzanov, D. Casanova, X. Feng, and A. I. Krylov, Quantifying charge resonance and multiexciton character in coupled chromophores by charge and spin cumulant analysis, *J. Chem. Phys.* **142**, 224104 (2015).
- [124] J. VandeVondele and J. Hutter, Gaussian basis sets for accurate calculations on molecular systems in gas and condensed phases, *J. Chem. Phys.* **127**, 114105 (2007).
- [125] S. Goedecker, M. Teter, and J. Hutter, Separable dual-space Gaussian pseudopotentials, *Phys. Rev. B* **54**, 1703 (1996).
- [126] C. Hättig, Optimization of auxiliary basis sets for RI-MP2 and RI-CC2 calculations: Core-valence and quintuple- $\zeta$  basis sets for H to Ar and QZVPP basis sets for Li to Kr, *Phys. Chem. Chem. Phys.* **7**, 59 (2005).
- [127] L. C. Bartel and B. Morosin, Exchange striction in NiO, *Phys. Rev. B* **3**, 1039 (1971).
- [128] S. Sasaki, K. Fujino, and Y. Takeuchi, X-ray determination of electron-density distributions in oxides, MgO, MnO, CoO, and NiO, and atomic scattering factors of their constituent atoms, *Proc. Jpn. Acad. Ser. B* **55**, 43 (1979).
- [129] O. Crisan and A.D. Crisan, Phase transformation and exchange bias effects in mechanically alloyed Fe/magnetite powders, *J. Alloys Compd.* **509**, 6522 (2011).
- [130] P. Pokhilko, C.-N. Yeh, and D. Zgid, Iterative subspace algorithms for finite-temperature solution of Dyson equation, *J. Chem. Phys.* **156**, 094101 (2022).
- [131] H. J. Monkhorst and J. D. Pack, Special points for Brillouin-zone integrations, *Phys. Rev. B* **13**, 5188 (1976).
- [132] Joachim Paier, Robin Hirschl, Martijn Marsman, and Georg Kresse, The Perdew–Burke–Ernzerhof exchange-correlation functional applied to the G2-1 test set using a plane-wave basis set, *J. Chem. Phys.* **122**, 234102 (2005).

- [133] Ravishankar Sundararaman and T. A. Arias, Regularization of the Coulomb singularity in exact exchange by Wigner-Seitz truncated interactions: Towards chemical accuracy in nontrivial systems, *Phys. Rev. B* **87**, 165122 (2013).
- [134] H. Shinaoka, J. Otsuki, M. Ohzeki, and K. Yoshimi, Compressing Green's function using intermediate representation between imaginary-time and real-frequency domains, *Phys. Rev. B* **96**, 035147 (2017).
- [135] Q. Sun, T. C. Berkelbach, N. S. Blunt, G. H. Booth, S. Guo, Z. Li, J. Liu, J. D. McClain, E. R. Sayfutyarova, S. Sharma, S. Wouters, and G. K. Chan, Pyscf: the python-based simulations of chemistry framework, *Wiley Interdiscip. Rev.: Comput. Mol. Sci.* **8**, e1340 (2017).
- [136] A. A. Rusakov and D. Zgid, Self-consistent second-order Green's function perturbation theory for periodic systems, *J. Chem. Phys.* **144**, 054106 (2016).
- [137] C.-N. Yeh, A. Shee, Q. Sun, E. Gull, and D. Zgid, Relativistic self-consistent *gw*: Exact two-component formalism with one-electron approximation for solids, *Phys. Rev. B* **106**, 085121 (2022).
- [138] A. Allouche, Gabedit-a graphical user interface for computational chemistry softwares, *J. Comput. Chem.* **32**, 174 (2011).
- [139] Persistence of vision (TM) raytracer.
- [140] A. H. Larsen, J. J. Mortensen, J. Blomqvist, I. E. Castelli, R. Christensen, M. Dułak, J. Friis, M. N. Groves, B. Hammer, C. Hargus, E. D. Hermes, P. C. Jennings, P. B. Jensen, J. Kermode, J. R. Kitchin, E. L. Kolsbjerg, J. Kubal, K. Kaasbjerg, S. Lysgaard, J. B. Maronsson, T. Maxson, T. Olsen, L. Pastewka, A. Peterson, C. Rostgaard, J. Schiøtz, O. Schütt, M. Strange, K. S. Thygesen, T. Vegge, L. Vilhelmsen, M. Walter, Z. Zeng, and K. W. Jacobsen, The atomic simulation environment—a Python library for working with atoms, *J. Phys.: Condens. Matter* **29**, 273002 (2017).
- [141] W. Setyawan and S. Curtarolo, High-throughput electronic band structure calculations: Challenges and tools, *Comput. Mater. Sci.* **49**, 299 (2010).
- [142] T. Archer, C. D. Pemmaraju, S. Sanvito, C. Franchini, J. He, A. Filippetti, P. Delugas, D. Puggioni, V. Fiorentini, R. Tiwari, and P. Majumdar, Exchange interactions and magnetic phases of transition metal oxides: Benchmarking advanced ab initio methods, *Phys. Rev. B* **84**, 115114 (2011).
- [143] J. B. Goodenough, Direct cation–cation interactions in several oxides, *Phys. Rev.* **117**, 1442

- (1960).
- [144] J. Kanamori, Superexchange interaction and symmetry properties of electron orbitals, *Journal of Physics and Chemistry of Solids* **10**, 87 (1959).
- [145] Y. R. Pei, Philip Anderson's superexchange model, <https://web.archive.org/web/20230323080536/https://courses.physics.ucsd.edu/2017/Fall/physics211a/specialtopic/1964.pdf>, 2017.
- [146] V. Halpern and D. Gabor, A generalized mechanism for superexchange, *Proceedings of the Royal Society of London. Series A. Mathematical and Physical Sciences* **291**, 113 (1966).
- [147] J.-Q. Chen, M.-J. Gao, and G.-Q. Ma, The representation group and its application to space groups, *Rev. Mod. Phys.* **57**, 211 (1985).
- [148] Alexei A. Kananenka, Emanuel Gull, and Dominika Zgid, Systematically improvable multi-scale solver for correlated electron systems, *Phys. Rev. B* **91**, 121111(R) (2015).
- [149] T. N. Lan, A. Shee, J. Li, E. Gull, and D. Zgid, Testing self-energy embedding theory in combination with GW, *Phys. Rev. B* **96**, 155106 (2017).
- [150] T. N. Lan, A. A. Kananenka, and D. Zgid, Communication: Towards ab initio self-energy embedding theory in quantum chemistry, *J. Chem. Phys.* **143**, 241102 (2015).
- [151] T. N. Lan, A. A. Kananenka, and D. Zgid, Rigorous ab initio quantum embedding for quantum chemistry using green's function theory: Screened interaction, nonlocal self-energy relaxation, orbital basis, and chemical accuracy, *J. Chem. Theory Comput.* **12**, 4856 (2016).
- [152] L. N. Tran, S. Isakov, and D. Zgid, Spin-unrestricted self-energy embedding theory, *J. Phys. Chem. Lett.* **9**, 4444 (2018).
- [153] Dominika Zgid and Emanuel Gull, Finite temperature quantum embedding theories for correlated systems, *New Journal of Physics* **19**, 023047 (2017).
- [154] A. A. Rusakov, S. Isakov, L. N. Tran, and D. Zgid, Self-energy embedding theory (SEET) for periodic systems, *J. Chem. Theory Comput.* **15**, 229 (2019).
- [155] C.-N. Yeh, S. Isakov, D. Zgid, and E. Gull, Electron correlations in the cubic paramagnetic perovskite  $\text{Sr}(\text{V}, \text{Mn})\text{O}_3$ : Results from fully self-consistent self-energy embedding calculations, *Phys. Rev. B* **103**, 195149 (2021).
- [156] A. Sadoc, R. Broer, and C. de Graaf, Role of charge transfer configurations in  $\text{LaMnO}_3$ ,  $\text{CaMnO}_3$ , and  $\text{CaFeO}_3$ , *J. Chem. Phys.* **126**, 134709 (2007).
- [157] J. Heyd, G. E. Scuseria, and M. Ernzerhof, Hybrid functionals based on a screened Coulomb

potential, J. Chem. Phys. **118**, 8207 (2003).